449 (1970).

[33]G. W. Cole, Jr., F. W. K. Firk, and T. W. Phillips, Phys. Letters 30B, 91 (1969); F. A. Hanser, Ph.D. thesis, Massachusetts Institute of Technology, 1967 (un-

published).

[34]N. G. Puttaswamy and D. Kohler, Phys. Letters 20, 288 (1966).

Two-Body Photodisintegration of He³ Between 40 and 150 MeV*

Nancy M. O'Fallon,† Louis J. Koester, Jr., and James H. Smith
University of Illinois at Urbana-Champaign, Urbana, Illinois 61801
(Received 24 January 1972)

In an experiment with semiconductor and scintillation counter telescopes we have measured the photodisintegration cross section of He³ at photon energies from 40 to 150 MeV and proton laboratory angles of 30, 60, 90, 120, and 135°.

I. INTRODUCTION

This paper describes an experimental measurement of the photodisintegration of He³ into a proton-deuteron final state for photon energies between 40 and 150 MeV. In the region from threshold to about 40 MeV, the two-body photodisintegration of He³ has been moderately well studied, as has the inverse reaction.[1-11] The general features are clear. The cross section rises rapidly from threshold to a peak of 1.0 mb at an energy of 11 MeV. It then tails off to about 0.2 mb at 40 MeV.

The angular distribution is best known from the inverse reaction.[10] Here again the features are clear. The angular distribution at 15 MeV is a $\sin^2\theta$ distribution pushed toward forward proton angles near 75° in the center-of-mass system. There is essentially no isotropic component (<1%).

Theories based on fairly simple ground-state wave functions that also fit electron scattering data are capable of describing the magnitude and energy dependence of the photodisintegration. The forward peaking in this low-energy region can be understood in terms of simple retardation effects caused by the size of the nuclear wave function.[12, 13]

At energies above 40 MeV, data are rather sparse. Fetisov, Gorbunov, and Varfolomeev[6] have measured the total cross section and angular distributions, but with very limited statistical accuracy. Picozza et al.[14] have measured 90° differential cross sections between 180 and 500 MeV. Didelez et al.[15] have measured the inverse reaction for the equivalent of 109-MeV photons and have a well-determined angular distribution.

This experiment was undertaken to investigate the energy and angular dependence of He³ photo-

disintegration from the region where it is well measured and moderately well understood in terms of photon interactions with nucleons described by a simple wave function up to meson threshold where other mechanisms for the interaction should become important.[16] An additional feature of interest is that detailed balance can be tested at 109 MeV where meson effects are not completely negligible.

II. EXPERIMENTAL APPARATUS AND PROCEDURE

A. Experimental Method and Arrangement

The experimental arrangement is shown in Fig. 1. The $He^3(\gamma, p)H^2$ reactions were produced by a 250-MeV bremsstrahlung beam incident on a low-temperature He³-gas target. Deuterons were counted in a counter telescope consisting of three transmission-type silicon semiconductor detectors followed by a plastic scintillator. Protons were detected in time coincidence by means of a telescope of four plastic scintillators. The photon beam was horizontal. The axes of the two detector telescopes were also horizontal and could be rotated independently about the target.

The solid angle was determined by the semiconductor detectors of the deuteron telescope. The plastic scintillators of the proton telescope were large enough to intercept all protons correlated with deuterons in the deuteron telescope throughout the entire energy interval. At each angular setting, therefore, cross-section measurements for all energies were carried out at the same time.

The energies of the deuterons and protons are determined by a combination of range and pulse

heights in their respective detectors. Because the energy information from the deuteron telescope is more precise than that from the proton detector, the angle and energy of the deuteron are used to determine the incident photon energy.

Two-body photodisintegration events are distinguished, first of all, by the requirement of time coincidence between the two particles produced. Next, the particle passing through the deuteron telescope is identified as a deuteron by the relative pulse heights in successive detectors. Finally, the particle in the proton telescope is assumed to be a proton and its energy is determined on this basis. This energy must bear the correct ratio to the deuteron energy for the event to be acceptable.

B. Equipment

(1) Target and beam. The target was mounted on the axis of a small rotating gun mount (Fig. 1). It was a slight modification of a target used previously by O'Fallon *et al.*[17] The lower part of its structure is shown in Fig. 2. The vertically mounted cylinder which contained the gaseous He³ was 2.86 cm in diameter and had a 0.0015-in. Mylar wall where the beam traversed it. It was in direct thermal contact with the liquid-He⁴ reservoir and was surrounded by three concentric radiation shields: one suspended from the liquid-He⁴ tank, one thermally isolated, and one at liquid-nitrogen temperature. These shields had 0.000 25-in. aluminum windows for the beam and outgoing particles and were very effective. The He⁴ evap-

oration rate was of the order 1 liter/day. A carbon resistance thermometer imbedded in the bottom of the target cylinder (Fig. 2) indicated that the He³ gas was at the same temperature (4.20 ±0.04°K) as the liquid helium. Once filled with He³ gas (at about 650 mm Hg), the target cylinder was sealed by a valve. An absolute pressure gauge on top of the assembly monitored the pressure. The liquid-helium temperature could vary with the atmospheric pressure, but the amount of gas in the beam could not change appreciably.

The density of He³ at this temperature and pressure is about 19% greater than one would expect for an ideal gas. The molar volume V may be computed from the equation

$$PV = RT(1 + B_V/V + C_V/V^2 + \cdots), \qquad (1)$$

where P is the pressure in atmospheres, $R = 82.06$ atm cm³/°K, and T is the absolute temperature in °K. The third virial coefficient, C_V is negligibly small, but $B_V = -54.0$ cm³/mole.[18] The result of Eq. (1), that $V = 339$ cm³/mole for 4.2°K and 650 mm Hg, agrees within 1% with values fitted to measurements by Kerr.[19]

The x-ray beam entered and left the target vacuum jacket through 0.005-in. Mylar windows. The beam was 4.14 cm high by 2.22 cm wide at the target. About 4 m downstream from the target the amount of irradiation was measured by a copper-plate ionization chamber. Both before and after the experiment, this chamber was compared, with a probable error of ±2.3%, with a
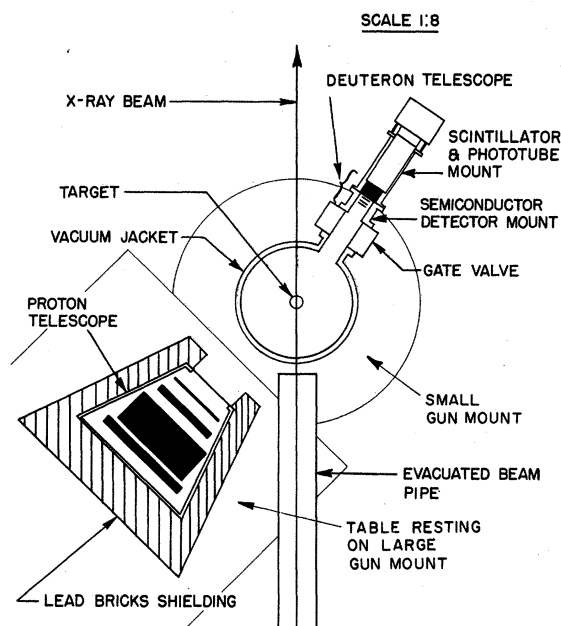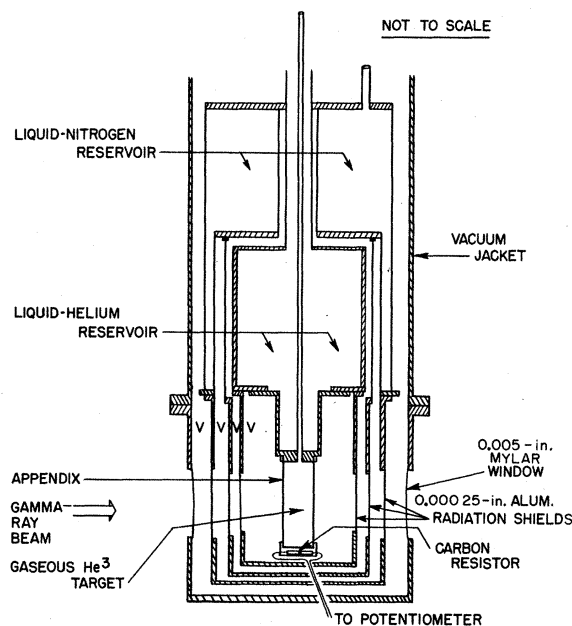

FIG. 1. Plan view of the experiment.

FIG. 2. Cutaway view of the low-temperature gas target.

ALL DIMENSIONS IN cm
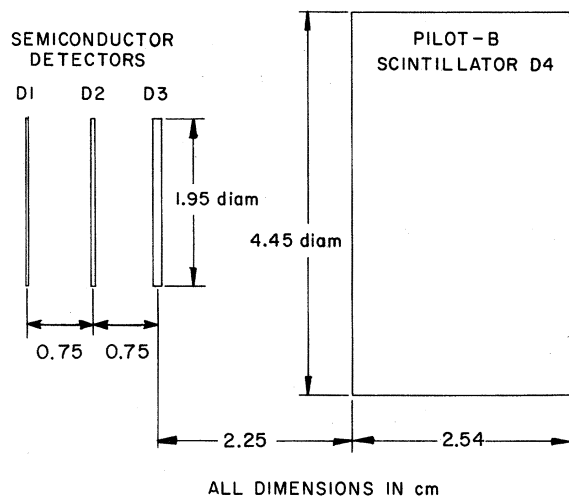
FIG. 3. Deuteron telescope. The totally depleted silicon detectors D1–D3 are transmission-mounted and have thicknesses of 217, 496, and 1000 μm, respectively. D4 is mounted on the face of the phototube.

calibrated quantameter borrowed from the Lawrence Berkeley Laboratory.[20]

(2) Deuteron telescope. The deuteron telescope was mounted directly on the target and shared the target vacuum. A 5-cm aperture gate valve between the target and telescope could be closed to remove the telescope for servicing. Deuteron observation angles were varied by rotating the entire target and telescope assembly mounted on the small gun mount. The telescope consisted of three circular, transmission-mounted, totally depleted silicon detectors followed by a cylindrical plastic scintillator (Fig. 3). This plastic scintillator was outside the vacuum, separated from it by a 0.005-in. Mylar window. The first semiconductor detector was 28.5 cm from the target center and was 3.00 cm² in area. The energy

limits of our measurement were chosen so that the deuterons would always penetrate through the first detector and stop somewhere in the telescope. The brass cylinder housing the detectors was water-cooled to keep reverse currents small.

The University of Illinois cyclotron was used to calibrate the semiconductor detectors with protons, deuterons, and α particles up to about 20 MeV. The detector responses proved to be proportional to the actual energy losses within 1% regardless of particle type or depth of penetration. A small amount of Po^{210} was deposited on the face of each semiconductor as a standard. The response to the 5.3-MeV α particles was checked periodically throughout the experiment.

The calibration of the plastic scintillator was more difficult. The light output of a plastic scintillator is not linear for heavily ionizing particles. In Fig. 4, the curves of scintillator light output vs particle energy for protons, deuterons, and tritons are taken from experimental results of Gooding and Pugh[21] and normalized to the observed pulse height of our most energetic proton stopping in the fourth deuteron counter. Other calibration points available through kinematics from our data and from a companion experiment with a He^4 target are plotted in Fig. 4 in satisfactory agreement with the curves. The linearity of the RCA 6655A phototube response was checked with a pulsed light source attenuated by calibrated filters. Its intensity and duration were similar to those of the scintillations.

(3) Proton telescope. The proton telescope was mounted on a larger gun mount concentric with the smaller one. Each time the deuteron angle was changed, the proton telescope was rotated independently to the correlated angle determined by kinematics. Protons emerged from the vacuum jacket through 0.005-in. Mylar windows. The five pairs of angular settings (in degrees) for the proton and
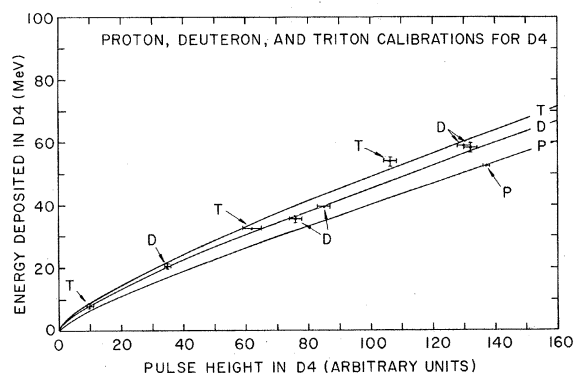

FIG. 4. Scintillator response curves used to calibrate D4. Solid curves are taken from experimental data of Ref. 20 and normalized to the observed pulse height of the most energetic proton stopping in D4.

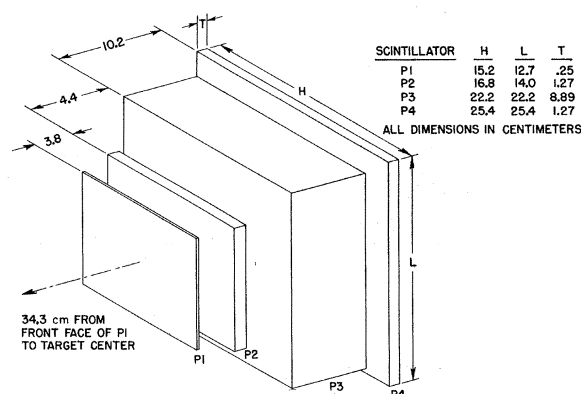| SCINTILLATOR	H	L	T
P1	15.2	12.7	.25
P2	16.8	14.0	1.27
P3	22.2	22.2	8.89
P4	25.4	25.4	1.27

ALL DIMENSIONS IN CENTIMETERS

FIG. 5. Proton telescope.

deuteron telescope, respectively, were (30, 142), (60, 106), (90, 75), (120, 47.5), and (135, 34.5).

Figure 5 is a perspective view of the four proton scintillators. The first scintillator was large enough to accept all protons correlated with deuterons in the semiconductor telescope for the energy interval 40–150 MeV. Lateral dimensions of the scintillators increased more rapidly than their distances from the target so that losses from Coulomb scattering could be neglected. The third scintillator, P3, was made thick enough to stop protons of the highest relevant energies. A particle penetrating into P4 could not be of interest to this experiment. The lowest-energy protons of interest penetrated P1 and stopped in P2, so they could be identified by relative pulse heights.

The thinner scintillators, P1, P2, and P4, were mounted in polished-aluminum enclosures viewed through air light pipes to avoid Čerenkov light from stray particles. Adding the signals from two phototubes, one above and one below each scintillator, made the response fairly independent of the point at which a particle entered the scintillator. Four phototubes on Lucite light pipes were used on P3.

No attempt was made to determine the energy response of the proton counters before the experiment, other than to adjust the phototube voltages for the desired interval of output signals. Once the correlated proton-deuteron (p, d) events were recorded, the calibration was accomplished by determining proton energies through kinematics from the measured deuteron energies. A single event would be subject to an uncertainty in the energy lost by the deuteron in escaping the target and in the angle of emission, but the median of a large number of events represented disintegrations at the target center as seen on the graphs in Fig. 6. These graphs consist of events in which a proton at 60° stops in the scintillator P2 or P3. The pulse heights in P2 and P3 are plotted vertically against the measured deuteron energy extrapolated to the target center. The energies of protons that just reach or just penetrate the scintillators are confirmed by range-energy relations, and the intermediate energies are known
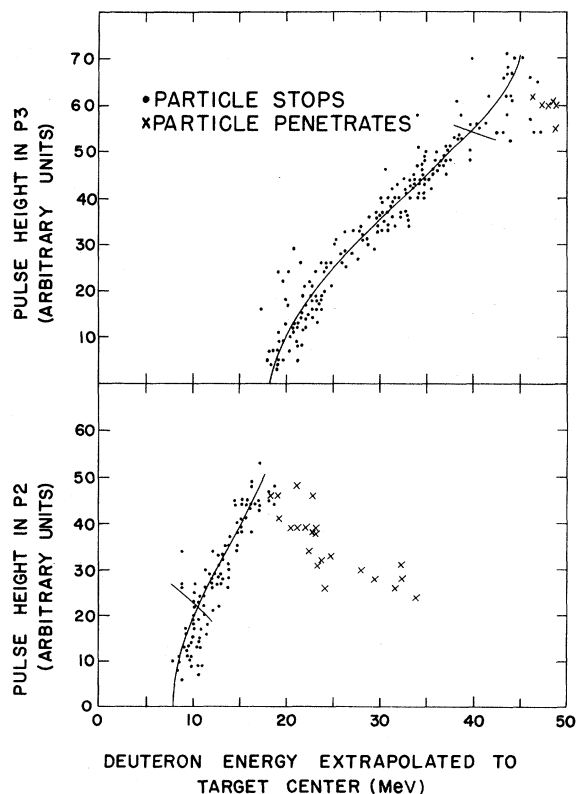

FIG. 6. Proton energy calibration. All protons of interest stop in P2 or P3. Cuts across the curves indicate the lower and upper limits of the energy interval used.
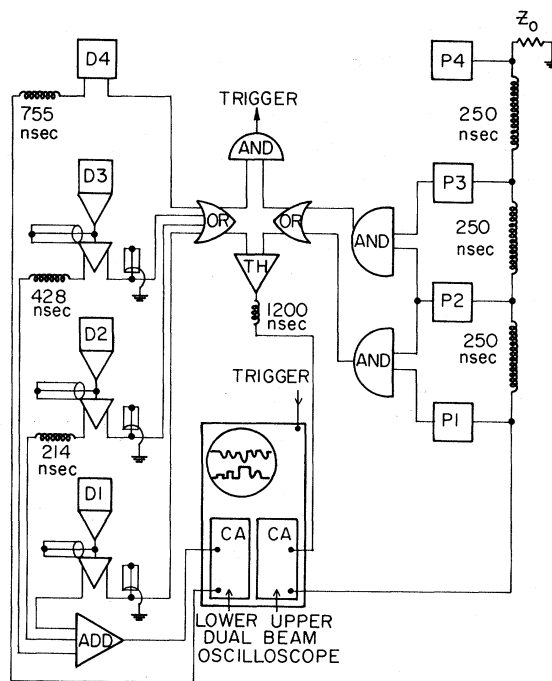

FIG. 7. Simplified block diagram of the electronics. D1–D3 are the semiconductor detectors and D4 is the plastic scintillator in the deuteron telescope. P1–P4 are the proton telescope scintillators. The OR and AND circuits perform the logical operations described in the text. The time-to-height circuit (TH) provides an analog output proportional to the delay between the proton and deuteron telescope signals. The unmarked triangles represent amplifiers. The Tektronix type CA plug-in units were set for algebraic addition of inputs. The indicated delays allowed the two sets of four analog signals to be displayed on the dual-beam oscilloscope.

from two-body kinematics. The line through the
middle of the point distribution is used to prepare
the proton energy calibration. The minimum
pulse height observable in P2 is determined by
coincidence requirements described below, but
it lies well below the lowest energy of interest to
the experiment.

   (4) Electronics. The electronic circuity (Fig. 7)
provided both the logic for recording events and
the analog pulse heights in all the detectors.
Modular fast logic circuits were used to trigger
the recording apparatus if the following condi-
tions were fulfilled: a coincidence within ±15
nsec between either P1 and P2 or P2 and P3 in the
proton telescope, and this output in ±30 nsec co-
incidence with any one of the deuteron detectors.
The allowance of these several possibilities took
account of the fact that the more energetic parti-
cles make larger pulses in the detectors farther
from the target. It permitted a higher threshold
setting on P1 to discriminate against the many
low-energy electrons there.

   The semiconductor signals were amplified
linearly by voltage amplifiers mounted directly
on the vacuum chamber and connected through
about 3 cm of miniature cable. The amplifier rise
time was about 3 nsec, but the fall time was about
5 μsec. These signals were clipped to a duration

long enough to assure complete charge collection,
75 nsec for D1, 100 nsec for D2, and 150 nsec for
D3. The clipping was done with a shorted line at
the grid inputs to a dual pentode inverter. The
linear output was taken from one of the anodes,
and the logic output, clipped again to 30 nsec
from the other anode.

   The linear signals were displayed on one trace
of a dual-beam oscilloscope (Tektronix 551) and
photographed when the sweep was triggered by the
above logic. The fast-voltage amplifiers were
used instead of the more usual charge-sensitive
amplifiers for two reasons:
(1) The fast wave form on the scope would show
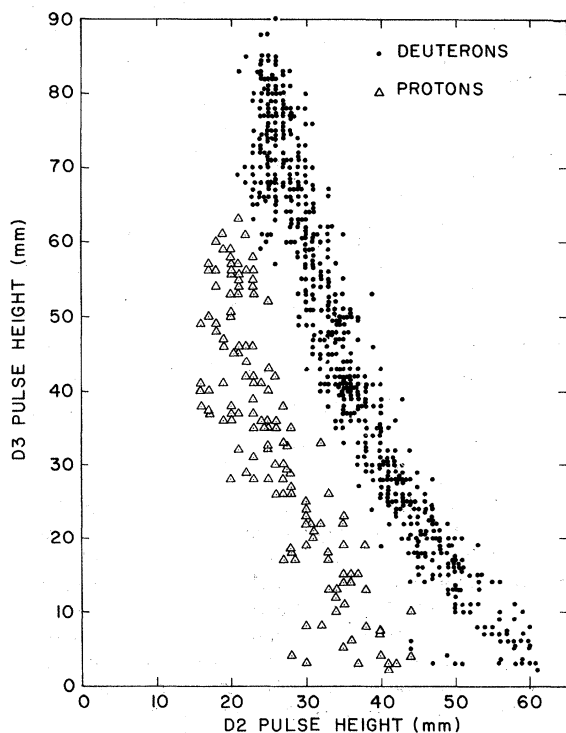any stray particles piling up, and

FIG. 8. Correlated pulse heights in D2 and D3 show-
ing the separation between protons and deuterons.
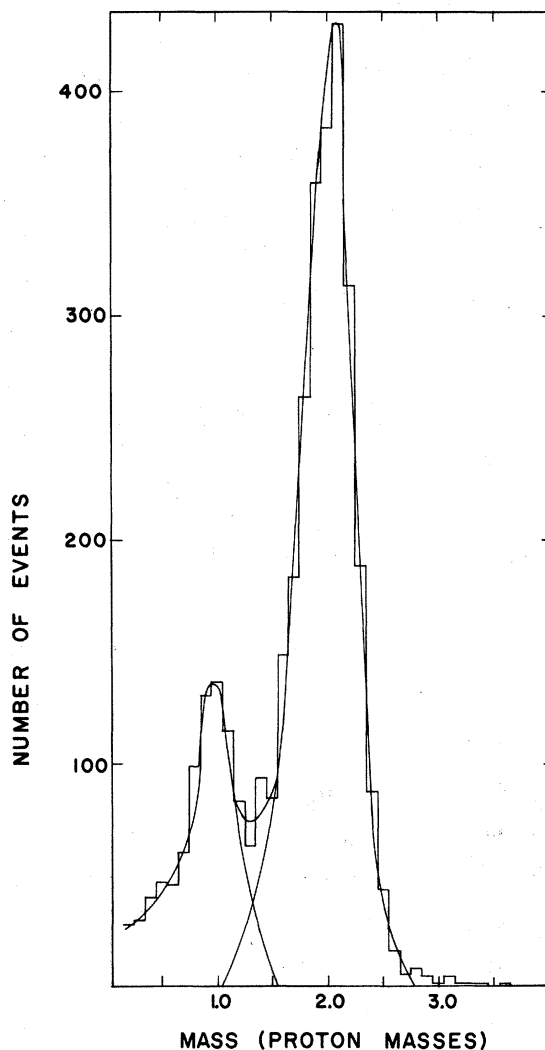

FIG. 9. Histogram of the mass parameter M_d com-
puted for particles in the deuteron telescope. Smooth
curves indicate proton and deuteron components. Deu-
terons predominate because of the angular-correlation
requirement.

(2) the fast rise time was needed for the coincidence logic and the timing could be observed on the scope as well.

The dynode signals from the proton telescope were displayed on the other trace of the dual-beam oscilloscope for each event. Thus each photograph contained, in addition to the run and frame number, the analog signal from each detector displayed in a particular location. The absence of signals at the wrong positions (or times) was good evidence of the validity of the events.

C. Background

The event signature on film was so nearly unique that background was not a problem. Nevertheless, certain checks were made to determine the empty-target background and random coincidences.

A series of empty-target runs was made at the most forward proton direction (30°) where spurious backgrounds were certainly the worst. The irradiation amounted to about 11% of that devoted to full target runs at this angular setting. At most, one event that might be called a He³ photodisintegration was observed. Since this would represent only about 1.5% background, no correction was made.

To check for random coincidences, a run was made with full target but with the deuteron signal arbitrarily delayed by 130 nsec. The amount of irradiation was sufficient to produce about 100 coincidences under normal conditions, but none occurred.

An additional item of information recorded on the film was the output of a time-to-amplitude converter measuring the overlap of the proton and deuteron logic signals. The master coincidence gate allowed a time variation of ±30 nsec between these two signals, whereas the observed time spread for good events was only from −15 to +8 nsec. Thus, even though this signal was not used as a criterion to select events, all the good events lay well within the timing limits.

This observed timing spread between protons and deuterons does not represent actual time-of-flight differences. It is caused mostly by rise-time variations in the semiconductor detectors. Not only does a small pulse take longer to reach threshold, but the actual pulse shape depends on the depth of penetration of the deuteron into the detector.

III. DATA ANALYSIS AND RESULTS

A. Identification of Events

The film containing the pulse-height information photographed from the oscilloscope was projected and measured manually. At this time all the pulse heights from one event were punched on an IBM card. Computer programs used this information to identify the particles, convert pulse heights to energies, and verify the kinematics of two-body photodisintegrations.

Deuterons were identified in the following manner. In Fig. 8, the energy deposited by each particle stopping in the third deuteron detector is plotted vertically against the energy lost in the preceding detector. Protons and deuterons fall on fairly well separated loci. Range energy relations predict curves that agree very well with the experimental points.

Simple empirical expressions were fitted to these curves for each pair of detectors. These expressions had all parameters fixed except one, M_d, representing the mass of the particle. The computer adjusted this one free parameter to fit the energy losses for a given event. The resulting values for M_d were distributed around 1 for protons, 2 for deuterons, and 3 for tritons (with He⁴ target only). Figure 9 shows a typical histogram of M_d values for a series of He³ runs. To be accepted as a deuteron, the particle in the deuteron telescope had to have a value for M_d between 1.4 and 2.7. This selection was made by the computer. The shape of the histogram (Fig. 9) indicated that about 1% of the true events were lost this way, so a correction was made to the results.

Once the deuteron was identified, the program used range and pulse height in the last detector to determine the energy E_d of the deuteron and the energy E_p of the coincident particle in the proton telescope, assumed to be a proton. It also computed the ratio $R = E_d/E_p$. E_d and E_p were determined on the assumption that the event came from the target center. The program also used the deuteron energy and angle to determine the photon energy E_{gam}.

The energy ratio R varied with angle and had a spread owing to the angular width of the detectors and the energy loss uncertainty in the target. Events were checked by comparing the printout of R with a graph of these kinematic limits. Approximately 2% of the events with acceptable M_d values were rejected in this test. This was the last criterion used for actual event rejection.

The determination of E_p and E_d is complicated by one problem not previously mentioned. Pulses from low-energy electrons occur frequently in the plastic scintillators and give rise to a kind of noise on the oscilloscope trace showing the pulse heights. If such an electron pulse is juxtaposed with a proton or deuteron pulse, only a very small error in energy is made. However, if such a pulse occurs later on the trace after the last real pulse and is erroneously recorded as an addition-

al pulse, the error in energy can be considerable. Because the semiconductor detectors are relatively thin, this source of noise is not a problem for them.

To remove this uncertainty, events in which a particle appeared to reach the deuteron scintillator D4 were recomputed with that fourth pulse arbitrarily set to zero. Likewise, particles apparently reaching the third or fourth proton detector were recomputed with the last pulse height set to zero. That computation was used which gave the best value for the proton-deuteron energy ratio, R. Only 2% of the final data events actually use the recomputed values. In all such cases, the final discarded pulse is very small. The diagnosis is thus confirmed.

One final note concerning event identification remains. Despite the poor particle mass resolution of the proton telescope, it was possible to identify events where a proton entered the deuteron detector and a deuteron entered the proton detector. What little analysis we did of these events showed the numbers to be consistent with our other data, but we believe them to be subject to much greater systematic error. Consequently, no such events appear in the final results. The solid angle was too small to measure three-body breakup.

B. Cross-Section Determination

The number of events Y produced by photons in the energy interval between k_1 and k_2 is

$$Y = \int_{k_1}^{k_2} \frac{d\sigma}{d\Omega} N(k) n\Omega dk ,$$

where $d\sigma/d\Omega$ is the differential cross section, n is the number of target nuclei per cm^2, Ω is the solid angle defined by the deuteron telescope and transformed to the center-of-mass system, and $\int_{k_1}^{k_2} N(k)dk = Q$ is the number of incident photons in this energy interval as determined by the Schiff[22] bremsstrahlung spectrum and the number of joules of irradiation registered by the monitor.

The target and counters were small enough that integration over their sizes was unnecessary to a precision of 0.5%. The cross section was evaluated by assuming it constant over the interval and solving

$$d\sigma/d\Omega = Y/n Q\Omega .$$

After the energy dependence of the cross section was observed, the mean energy of the interval at which to plot the point was found by integration:

$$K \equiv \langle k \rangle = \int_{k_1}^{k_2} k N(k) \frac{d\sigma}{d\Omega} dk \bigg/ \int_{k_1}^{k_2} N(k) \frac{d\sigma}{d\Omega} dk .$$

The approximation $N(k) \sim 1/k$ is adequate for this purpose.

The energies k_1 and k_2 are the values of E_{gam} at the limits of the bin in which the number of events, Y, was collected. These bins were chosen wide enough to maintain reasonable statistical accuracy and to straddle the boundaries between the detectors in the telescopes. The uncertainty in the energy assignment of a given event is of the same order of magnitude as the bin width at the lower energies but is much smaller at the higher energies.

The observed values of Y were subject to adjustment for the following deficiencies:

(1) Events not read from the film because they had occurred too soon after another event for the film advance to be completed. This correction, which could be determined very precisely because the spoiled records were all on the film, varied only with the angular setting (i.e., the over-all trigger rate). It amounted to 1.9% at the least affected angle and 7.6% at the most.

(2) Changes in the defining solid angle of the experiment. The proton telescope was large enough to insure that the semiconductor defined the solid angle. Since the three semiconductors were of equal area, however, the solid angle decreased by 11.7% in going from the first to the third detector. This is not a correction but rather a definition of the solid angle and is well understood.

(3) Deuteron "masses" falling slightly outside the acceptance interval (see above and Fig. 8). A correction of 1% was made for this effect.

(4) Particle interactions in the detectors. Approximately 1% of the deuterons[23] would interact with the silicon nuclei in the detectors. If these were (d, p) or (d, n) reactions, the computer mass value for the interacting deuteron might be wrong. About 1% of the protons would make $C^{12}(p, pn)C^{11}$ reactions in the scintillators.[24] In such a case, the proton energy determination would be spoiled and the event rejected because the ratio $R = E_d/E_p$ was wrong (see above). Elastic scattering, $C^{12}(p, pp)B^{11}$ reactions, etc. are unlikely to affect the analysis. Single and multiple Coulomb scattering losses were estimated to be negligible. No correction for interactions has been made.

C. Presentation of Results

The uncorrected data are listed in Table I. All results are given in terms of the proton direction because traditionally the lighter outgoing particle is emphasized, even though the deuteron telescope determined the solid angle. In Table II the final differential cross sections in the center-of-

TABLE I. Experimental data.

Incident photon energy interval k_1 to k_2 (MeV)	Number of incident photons per joule of irradiation (units of 10^9)	30°	60°	90°	120°	135°
			Number of good p-d events at the proton telescope angle specified			
40–45	3.50	148	472	915	246	207
45–50	3.07	86	318	762	166	159
50–55	2.73	68	265	488	141	127
55–60	2.45		199		102	
55–65	4.67	126		696		207
60–70	4.24		234		121	
65–75	3.87	66		378		70
70–80	3.55		153		62	
75–90	4.74	59		213		88
80–90	3.04		113		58	
90–110	4.98	44	104	169	73	62
110–130	3.97	14	56	116	29	44
130–150	3.30	11	28	68	22	13
Totals		622	1942	3805	1020	977
Number of joules of irradiation		232	525	1349	551	735

mass system are presented. The incident photon energy is given in the laboratory system. The proton center-of-mass angles vary monotonically with increasing energy between the given limits. Errors shown are purely statistical.

We believe that our combined systematic errors are probably less than 7%. They are:

(a) A 2.3% uncertainty in the monitor calibration.

(b) A 2.5% uncertainty in the number of nuclei in the target. This comes about because of possible non-uniform temperatures and uncertainties in target size at liquid-helium temperatures.

(c) A 1.0% error in the actual number of events. A 1.0% correction has been made for good events with M_d outside the specified limits. This correction is very unceratin, and we attribute a 1% error to it and other possible mistakes in event identification.

(d) A 1.5% error for nuclear interactions of particles. We made no correction for these in our data; if a correction were made for them, our cross sections would be raised to this extent.

(e) A 1.0% error owing to finite energy resolution. If a cross section falls rapidly with energy,

TABLE II. Differential cross sections in the c.m. system. The two angles at the head of each column are mean values at 40 and 150 MeV, respectively. The actual mean proton angle in each photon energy interval may be obtained to sufficient accuracy by a linear interpolation against photon energy.

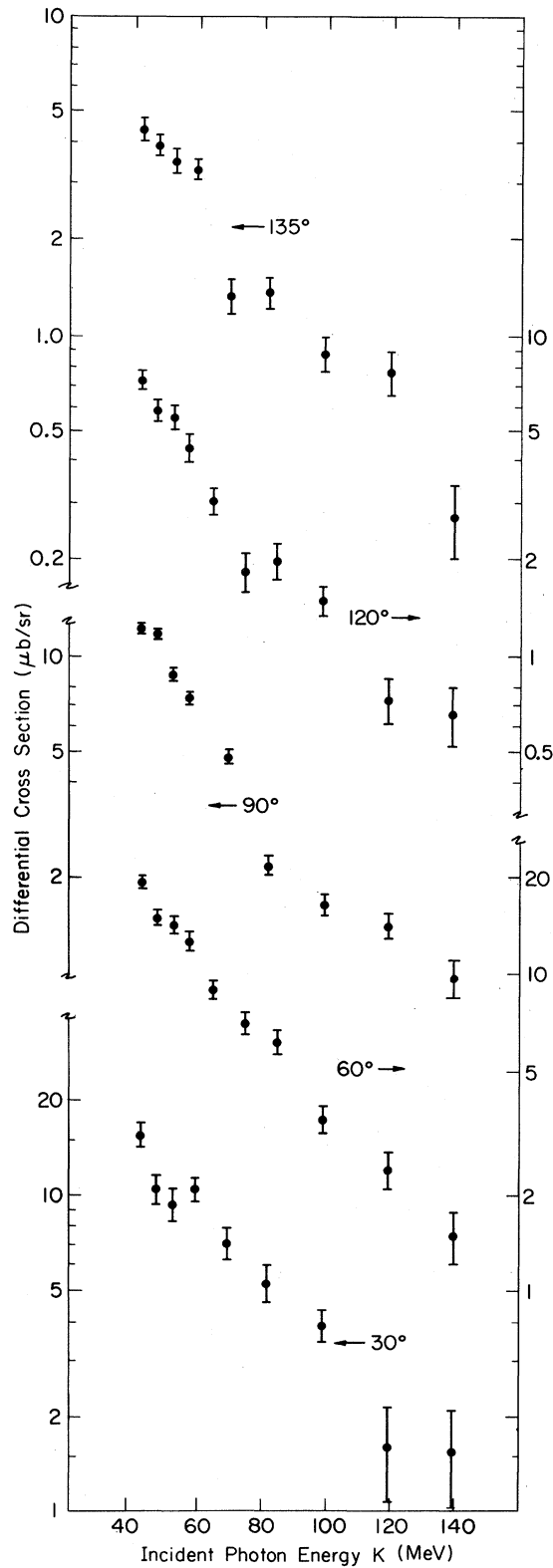| Incident photon energy (lab system) (MeV)	33.5–29.6°	67.2–61.5°	98.0–92.3°	127.1–122.7°	141.1–137.7°
	$d\sigma/d\Omega$ (c.m. system) in μb/sr at c.m. proton angle specified				
42.4	15.5 ± 1.3	19.23 ± 0.88	12.06 ± 0.40	7.29 ± 0.47	4.42 ± 0.37
47.4	10.4 ± 1.1	14.82 ± 0.83	11.63 ± 0.42	5.86 ± 0.46	3.94 ± 0.31
52.4	9.4 ± 1.1	14.12 ± 0.86	8.75 ± 0.40	5.57 ± 0.47	3.52 ± 0.31
57.4		12.53 ± 0.89	7.40 ± 0.28	4.46 ± 0.45	
59.6	10.4 ± 0.9				3.31 ± 0.23
64.6		8.78 ± 0.57		3.04 ± 0.28	
69.6	7.07 ± 0.79		4.77 ± 0.24		1.33 ± 0.16
74.7		6.92 ± 0.54		1.83 ± 0.26	
81.8	5.30 ± 0.72		2.17 ± 0.15		1.37 ± 0.15
84.7		6.06 ± 0.52		1.98 ± 0.26	
99.0	3.88 ± 0.46	3.47 ± 0.34	1.63 ± 0.13	1.49 ± 0.16	0.88 ± 0.11
119.2	1.60 ± 0.53	2.41 ± 0.32	1.40 ± 0.13	0.73 ± 0.12	0.77 ± 0.12
139.3	1.56 ± 0.53	1.49 ± 0.28	0.99 ± 0.12	0.66 ± 0.14	0.27 ± 0.07

FIG. 10. Differential cross sections measured at the five proton angles of this experiment versus incident photon energy.
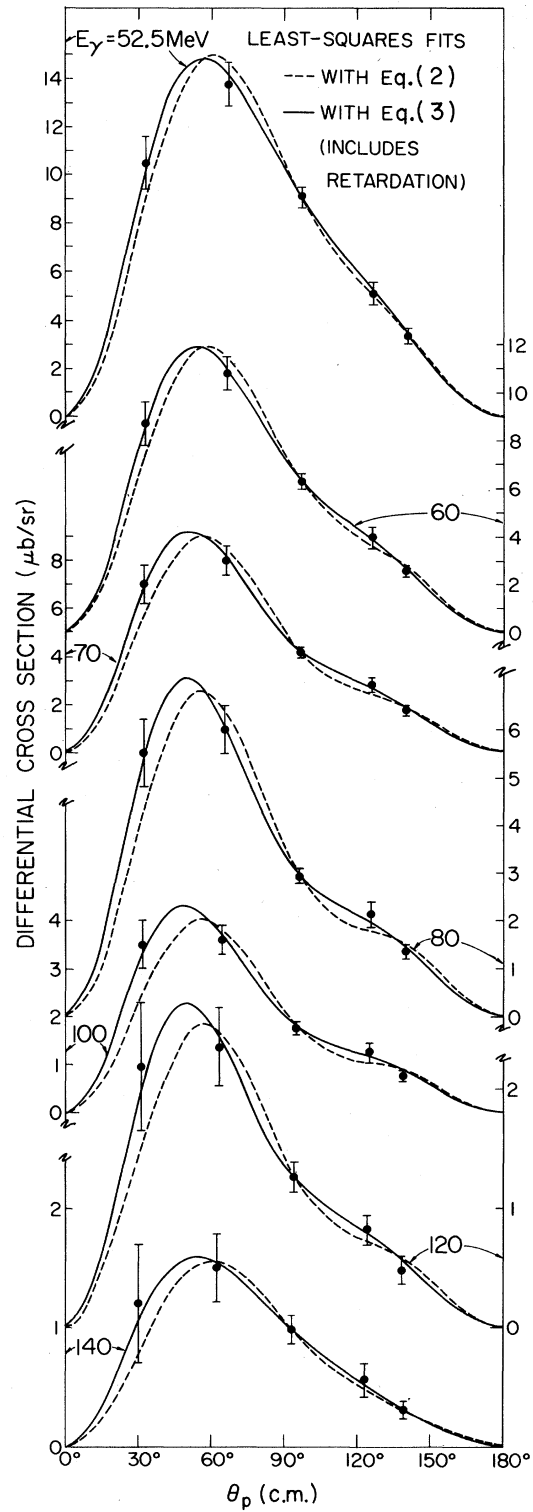
FIG. 11. Angular distributions for seven incident photon energy intervals centered at the energies indicated in MeV. The points are obtained by interpolation of Fig. 9. The curves are least-squares fits with Eq. (2) (dotted) and Eq. (3) (solid).

and if there is an uncertainty in the energy, more events enter an energy interval from below than leave it from above. We cannot make a reliable estimate of this effect, but we believe it to be less than 1%.

(f) A 3.0% error from a systematic error in particle energies. A systematic 1.0% error in the energy of an event causes roughly a 3.0% error in cross section because of the rapid decrease of cross section with energy. We believe a systematic error of this magnitude is possible.

The sum of all these errors is 11.3%. Their root mean square is 5.0%. We believe a fair value to assign to our systematic errors is 7%.

The cross sections of Table II are plotted vs energy in Fig. 10. Smooth curves through these points are used to interpolate values for the angular distributions shown in Fig. 11. Least-square fits to these angular distributions have been made with several functional forms. The most popular of these,

$$\frac{d\sigma}{d\Omega} = A \sin^2\theta (1 + B\cos\theta + C\cos^2\theta), \qquad (2)$$

where θ is the c.m. system proton angle, is compared with our results in Fig. 11. As this figure shows, a considerably better fit (smaller values of χ^2) is obtained with the form

$$\frac{d\sigma}{d\Omega} = \frac{a\sin^2}{(1 - \beta\cos\theta)^2} (1 + b\cos\theta + c\cos^2\theta), \qquad (3)$$

where β is the ratio of the c.m. system proton velocity to the speed of light. Addition of an isotropic term lowers the confidence level and, consequently, does not improve the fits. The $\cos^2\theta$ term cannot be dropped without spoiling the fits. Values of our angular-distribution parameters are given in Table III.

The retardation factor $(1 - \beta\cos\theta)^{-2}$ appearing in Eq. (3) above is suggested by an intutitive treat-

ment of the Born approximation for photoproduction.[25] Consider the crude matrix element for photoproduction proportional to

$$\int e^{-i\vec{p}\cdot\vec{r}} i(\vec{A}\cdot\vec{\nabla})\Psi(r)d\vec{r},$$

which may be manipulated to be $(\vec{\epsilon}\cdot\vec{p})\int e^{-i(\vec{p}-\vec{k})\cdot\vec{r}} \times \Psi(r)d\vec{r}$. Here we set $\hbar = c = 1$, so that $\vec{p}$ is the momentum or wave vector of the outgoing proton, $\vec{k}$, the same for the incident photon, and k its energy as used earlier in this section. The incoming photon plane wave is $\vec{A} = \vec{\epsilon}\,e^{i\vec{k}\cdot\vec{r}}$, where $\vec{\epsilon}$ is the polarization vector of the photon. The final proton state is taken to be a plane wave.

Now replace the initial proton state by its asymptotic value $r^{-1}e^{-\alpha r}$, where $\alpha^2 = 2mB$, m is the proton mass, and B is the binding energy. This factor r^{-1} in the initial state is characteristic of a potential of finite range and does not appear in the case of the atomic Coulomb potential. This factor is mainly responsible for the second power of $(1 - \beta\cos\theta)$ in the nuclear photodisintegration rather than the fourth power as in the atomic photoeffect.

The factor $\vec{\epsilon}\cdot\vec{p}$ when suitably averaged, is responsible for the $\sin\theta$ factor multiplying the entire matrix element. It can be ignored in this discussion. Then the above matrix element is proportional to

$$\int r^{-1}\exp[-i(\vec{p}-\vec{k})\cdot\vec{r} - \alpha r]d\vec{r}.$$

The value of this well-known integral is proportional to $(\alpha^2 + k^2 + p^2 - 2kp\cos\theta)^{-1}$, where the substitution $|p - k|^2 = p^2 + k^2 - 2pk\cos\theta$ has been made for the square of the momentum transfer.

With the substitution $\alpha^2 = 2mB$ and $p^2 = 2mT + T^2$, where T is the proton kinetic energy, the matrix element becomes $(2mB + 2mT + T^2 + k^2 - 2kp\cos\theta)^{-1}$. Since $B + T = k$, the photon energy, the matrix ele-

TABLE III. Angular-distribution coefficients and total cross sections.

Incident photon energy (MeV)	Expression (2), "traditional"			Expression (3) with retardation			
	A (μb/sr)	B	C	a (μb/sr)	b	c	σ_T (μb)
42.4	14.6 ± 0.4	1.11 ± 0.13	1.13 ± 0.22	14.2 ± 0.4	0.51 ± 0.11	0.90 ± 0.22	153 ± 8
47.4	12.5 ± 0.4	1.11 ± 0.14	1.14 ± 0.24	12.2 ± 0.4	0.46 ± 0.11	0.86 ± 0.23	130 ± 7
52.5	10.5 ± 0.4	1.18 ± 0.17	1.23 ± 0.29	10.2 ± 0.4	0.48 ± 0.14	0.92 ± 0.28	110 ± 6
60	7.45 ± 0.31	1.41 ± 0.20	1.65 ± 0.33	7.19 ± 0.32	0.60 ± 0.16	1.30 ± 0.32	84 ± 4
70	5.07 ± 0.21	1.64 ± 0.23	2.05 ± 0.37	4.83 ± 0.22	0.72 ± 0.19	1.66 ± 0.36	61 ± 4
80	3.56 ± 0.16	1.81 ± 0.27	2.38 ± 0.44	3.37 ± 0.16	0.76 ± 0.22	1.94 ± 0.44	45 ± 3
100	2.09 ± 0.13	1.81 ± 0.32	2.41 ± 0.57	1.98 ± 0.13	0.67 ± 0.25	1.95 ± 0.57	27 ± 2
109	1.75 ± 0.13	1.86 ± 0.40	2.60 ± 0.72	1.65 ± 0.13	0.62 ± 0.30	2.08 ± 0.70	23 ± 2
120	1.44 ± 0.13	1.63 ± 0.46	2.04 ± 0.84	1.37 ± 0.13	0.49 ± 0.34	1.51 ± 0.78	18 ± 2
140	1.06 ± 0.12	1.31 ± 0.56	1.16 ± 0.90	1.04 ± 0.12	0.27 ± 0.38	0.62 ± 0.76	11 ± 2

ment becomes

$$(2mk + 2T^2 + 2BT + B^2 - 2kp\cos\theta)^{-1}$$

$$= (2mk + 2Tk + B^2 - 2kp\cos\theta)^{-1}$$

$$= \left[2k(m + T)\left(1 - \frac{p}{m + T}\cos\theta + \frac{B^2}{2k(m + T)} \right) \right]^{-1}.$$

The last term is about 10^{-4} and may be neglected. Since $p(m + T)^{-1} = \beta$, the matrix element is proportional to $(1 - \beta\cos\theta)^{-1}$ and the cross section to $(1 - \beta\cos\theta)^{-2}$.

This retardation factor is highly singular even for rather small values of β. It pays to remove it before fitting the more dynamical terms with a polynomial.

IV. COMPARISON WITH OTHER EXPERIMENTS

Figure 12 compares the 90° cross sections found in this experiment with those found by other workers at lower and higher energies. In order to translate our measured cross sections, which were taken near 90°, to exactly 90° in the c.m. system, we adjusted each data point to 90° (c.m. system) according to the shape of the angular distribution. On this logarithmic scale, at least, the agreement appears good.

Figure 13 shows our total cross sections computed by integrating Eq. (3) and substituting values of a, b, and c from Table III. The data of Fetisov, Gorbunov, and Varfolomeev[6] are plotted for comparison.

A comparison of our data to those from the inverse reaction of Didelez et al.[15] at 109 MeV is shown in Fig. 14. Some of our points appear about 10% too low, but the angular distributions give no grounds for suspecting any failure of time-reversal invariance.

Values of the angular-distribution parameters B, C, b, and c determined by a least-squares fitting of our cross sections with expressions (2) and (3) are listed in Table III. The B and C val-

FIG. 12. Comparison of 90° cross sections from this experiment with other measurements. See Refs. 3–5, 7, 14.
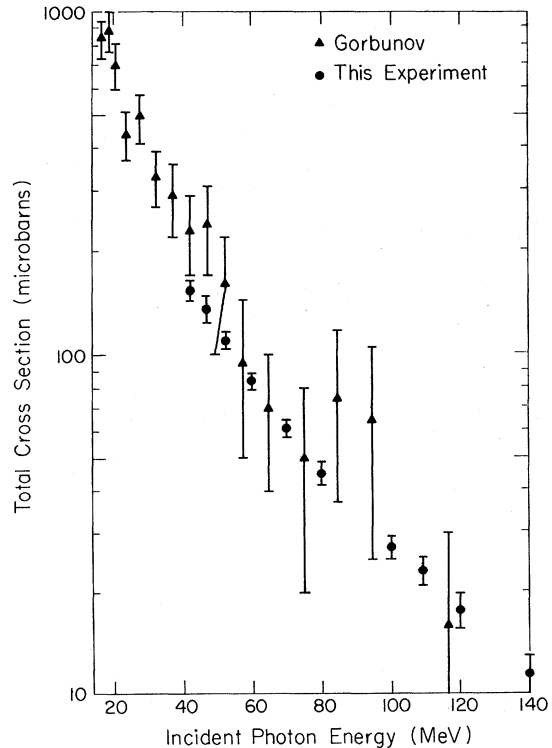
FIG. 13. Comparison of total cross sections from this experiment with those of Ref. 6.

ues are plotted in Fig. 15 along with those found by other experimenters, mostly at lower energies. The trends in the data agree all the way from the lowest energies midway through our data.

The fit to our data that uses a retardation term is consistently better than that which uses only dipole and quadrupole terms (Fig. 11). This argues that in the energy region of our experiment, theoretical treatments based on multipole expansions are probably not very useful. A full plane-wave treatment may be required. However, Carron[26] at 60 MeV and Didelez et al.[15] at 109 MeV have attempted different versions of such a plane-wave calculation, and both find theoretical angular distributions much too highly peaked forward to fit the data. It is unclear just what feature of the theoretical treatment is inadequate. Indeed, at our highest energies the coefficients B and C appear to be increasing only slowly with energy — or even to be decreasing. A new interaction mechanism is probably responsible for this reversal in trend, an interaction almost certainly involving virtual production of pions. Whether such an interaction is important even at the lower

energies of 60 and 109 MeV remains to be determined.

V. CONCLUSIONS AND SUMMARY

We have measured the energy and angular distributions of the reaction $He^3(\gamma, p)H^2$ from 40 to 150 MeV. The experimental results continue the trends evident at lower energies. The total cross

FIG. 15. Angular-distribution coefficients B (a) and C (b) in Eq. (2). Symbols are as follows: ●, this experiment; ▲, Ref. 8; ▼, Ref. 6; ×, Ref. 11; ■, Ref. 9; †, Ref. 1. Curves are theoretical, Ref. 12.
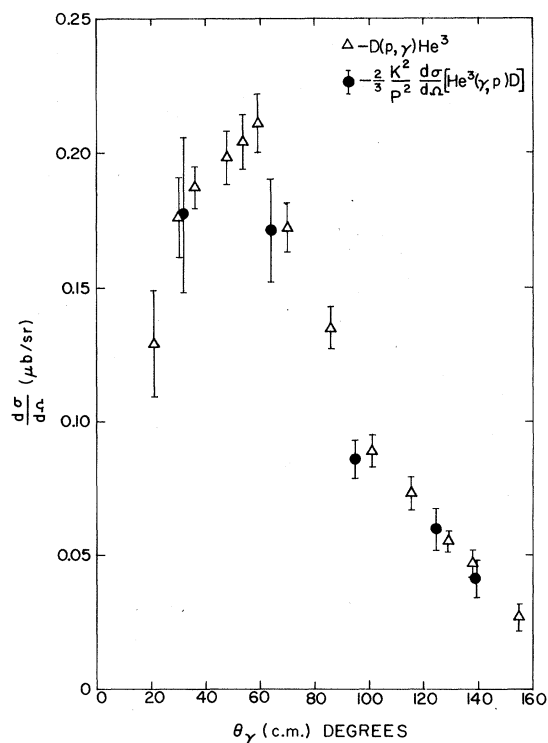

FIG. 14. Comparison with the inverse reaction (Ref. 15). Cross sections from this experiment are converted to those for the proton-capture reaction by detailed balancing. All cross sections are absolute, not normalized. The inverse reaction was performed with 156-MeV incident protons.
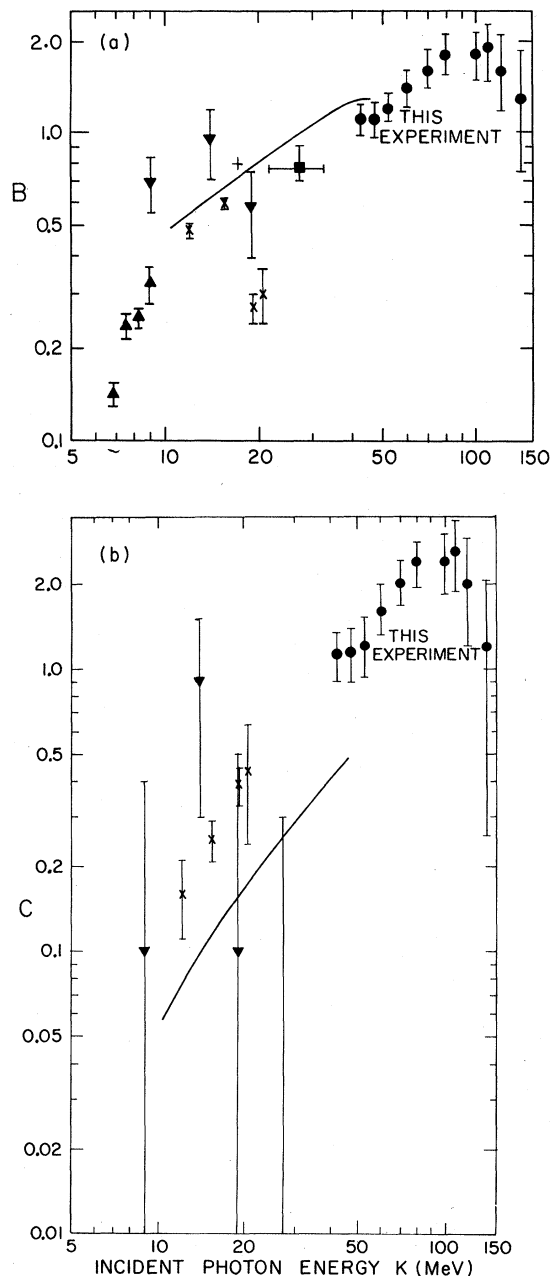
section continues to fall. The angular distributions peak more and more forward, except at our highest energies where there is some evidence in the angular distribution that a new mechanism is appearing. At 109 MeV the results agree with measurements of the inverse reaction, and therefore give no evidence against time-reversal invariance.

No present theory gives an adequate description of both the total cross section and angular distribution throughout this energy region. It appears somewhat unlikely that any theory based on a simple point interaction of the electromagnetic field with single nucleons described by a simple wave function will be found to do so.

ACKNOWLEDGMENTS

*Work supported in part by the National Science Foundation Grant No. GP 2799.

†Present address: University of Missouri - St. Louis, St. Louis, Missouri 63121.

[1] L. Cranberg, Bull. Am. Phys. Soc. 3, 173 (1958).

[2] C. M. Griffiths, E. A. Larson, and L. P. Robertson, Can. J. Phys. 40, 402 (1962).

[3] J. B. Warren, K. L. Erdman, L. P. Robertson, D. A. Axen, and J. R. MacDonald, Phys. Rev. 132, 1691 (1963).

[4] E. Finckh, R. Kosiek, K. H. Lindenberger, U. Meyer-Berkhout, N. Nücker, and K. Schlüpmann, Phys. Letters 7, 271 (1963).

[5] B. L. Berman, L. J. Koester, Jr., and J. H. Smith, Phys. Rev. 133, B117 (1964).

[6] V. N. Fetisov, A. N. Gorbunov, and A. T. Varfolomeev, Nucl. Phys. 71, 305 (1965).

[7] J. R. Stewart, R. C. Morrison, and J. S. O'Connell, Phys. Rev. 138, B372 (1965).

[8] W. Wölfli, R. Bösch, J. Lang, R. Müller, and P. Marmier, Phys. Letters 22, 75 (1966).

[9] H. Bock and H. Walenta, Z. Physik 238, 56 (1970).

[10] B. D. Belt, C. R. Bingham, M. L. Halbert, and A. van der Woude, Phys. Rev. Letters 24, 1120 (1970).

[11] A. van der Woude, M. L. Halbert, and C. R. Bingham, Phys. Rev. Letters 26, 909 (1971).

[12] G. M. Bailey, G. M. Griffiths, and T. W. Donnelly, Nucl. Phys. A94, 502 (1967).

[13] I. M. Barbour and A. C. Phillips, Phys. Rev. C 1, 165 (1970).

[14] P. Picozza, C. Schaerf, R. Scrimaglio, G. Goggi, A. Piazzoli, and D. Scannicchio, Nucl. Phys. A157, 190 (1970).

[15] J. P. Didelez, H. Langevin-Joliot, Z. Marić, and V. Radojević, Nucl. Phys. A143, 602 (1970).

[16] R. R. Wilson, Phys. Rev. 86, 125 (1952).

[17] J. R. O'Fallon, L. J. Koester, Jr., J. H. Smith, and A. I. Yavin, Phys. Rev. 141, 889 (1966).

[18] American Institute of Physics Handbook (1963), 2nd ed., pp. 4–158.

[19] E. C. Kerr and R. H. Sherman, in Proceedings of the Eleventh International Conference on Low Temperature Physics, St. Andrews, Scotland, 1968, edited by J. F. Allen, D. M. Finlayson, and D. M. McCall (St. Andrews University, St. Andrews, Scotland, 1969), and additional unpublished results.

[20] A. O. Hanson, private communication.

[21] T. J. Gooding and H. G. Pugh, Nucl. Instr. Methods 7, 189 (1960).

[22] L. I. Schiff, Phys. Rev. 83, 252 (1951).

[23] M. A. Melkanoff, T. Sawada, and N. Cindro, Nucl. Data A2, 263 (1966).

[24] H. J. Kim, W. T. Milner, and F. K. McGowan, Nucl. Data A2, 1 (1966).

[25] This argument is based on conversations with R. Schult.

[26] N. J. Carron, Phys. Rev. 168, 1095 (1968).